Applied Energy 189 (2017) 31–43

Contents lists available at ScienceDirect

Applied Energy

journal homepage: www.elsevier.com/locate/apenergy

A thermophysical battery for storage-based climate control

Shankar Narayanan [a,1], Hyunho Kim [a], Ari Umans [a], Sungwoo Yang [a], Xiansen Li [a], Scott N. Schiffres [a,2], Sameer R. Rao [a], Ian S. McKay [a,3], Carlos A. Rios Perez [b], Carlos H. Hidrovo [b], Evelyn N. Wang [a,*]

[a] Department of Mechanical Engineering, Massachusetts Institute of Technology, 77 Massachusetts Avenue, Cambridge, MA 02139, USA
[b] Department of Mechanical and Industrial Engineering, Northeastern University, 360 Huntington Ave., Boston, MA 02115, USA

HIGHLIGHTS

- The concept of a thermophysical battery for storing thermal energy is demonstrated.
- The battery provides heating and cooling for stationary and mobile applications.
- Energy storage mechanisms: adsorption-desorption and evaporation-condensation.
- Max. heating: 103 W/l and 65 W/kg; Max. Cooling: 78 W/l and 49 W/kg.
- Novel adsorbents further enhance performance for a compact and lightweight system.

GRAPHICAL ABSTRACT

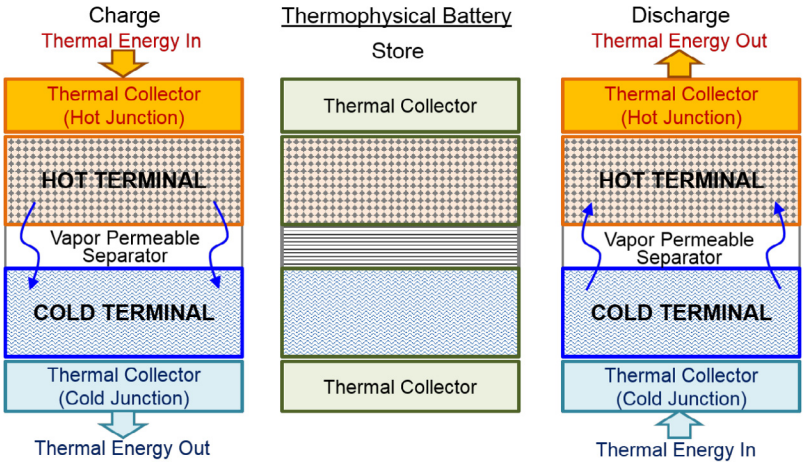

ARTICLE INFO

Article history:
Received 9 August 2016
Received in revised form 30 November 2016
Accepted 1 December 2016
Available online 22 December 2016

Keywords:
Thermal energy storage
Climate control
HVAC
Adsorption
Air conditioning

ABSTRACT

Climate control applications in the form of heating and cooling account for a significant portion of energy consumption in buildings and transportation. Consequently, improved efficiency of climate control systems can significantly reduce the energy consumption and greenhouse gas emissions. In particular, by leveraging intermittent or continuous sources of waste heat and solar energy, thermally-driven energy storage systems for climate control can play a crucial role. We demonstrate the concept of a thermophysical battery, which operates by storing thermal energy and subsequently releasing it to provide heating and cooling on demand. Taking advantage of the adsorption-desorption and evaporation-condensation mechanisms, the thermophysical battery can be a high-power density and rechargeable energy storage system. We investigated the thermophysical battery in detail to identify critical parameters governing its overall performance. A detailed computational analysis was used to predict its cyclic performance when exposed to different operating conditions and thermodynamic cycles. In addition, an experimental test bed was constructed using a contemporary adsorptive material, NaX-zeolite, to demonstrate this concept and deliver average heating and cooling powers of 900 W and 650 W, respectively. The maximum power densities and specific powers observed were 103 W/l and 65 W/kg for heating, and 78 W/l and 49 W/kg for cooling, respectively, making the thermophysical battery competitive with the state-of-the-art climate control systems that provide relatively lower power densities. Additionally, with

* Corresponding author.
E-mail addresses: narays5@rpi.edu (S. Narayanan), enwang@mit.edu (E.N. Wang).
[1] Present address: Department of Mechanical Aerospace and Nuclear Engineering, Rensselaer Polytechnic Institute, 110 8thStreet, Troy, NY 12180, USA.
[2] Present address: Department of Mechanical Engineering, State University of New York at Binghamton, 4400 Vestal Parkway East, Binghamton, NY 13902, USA.
[3] Present address: Department of Chemical Engineering, Stanford University, 443 Via Ortega, Stanford, CA 94305, USA.

http://dx.doi.org/10.1016/j.apenergy.2016.12.003

further opportunities for development and innovation, especially in synthesizing novel adsorptive materials, the thermophysical battery can achieve significantly higher power densities. With its ability to function using thermal energy input while being compact and lightweight, the thermophysical battery offers an option to address the energy challenges associated with the rising demand for climate control.

1. Introduction

Current trends in energy use indicate a substantial increase in global oil demand and greenhouse gas emissions by 2050. Climate control in the form of heating and cooling in households, industrial and commercial buildings, accounts for more than seventy-five percent of the total energy utilization [1]. Consequently, buildings alone account for almost a third of the energy consumption globally and are a significant source of carbon-dioxide emission [1]. Meanwhile, the impact of climate control on petroleum consumption in the transportation sector is also significant, posing several global problems due to costs, oil security [2,3] and emission of greenhouse gases and pollutants [4]. Therefore, to address the rise in energy consumption and emissions, efficient and environmentally sustainable systems for climate or temperature control is desirable. Additionally, for mobile applications such as vehicles, a compact and lightweight strategy is desirable.

Energy-efficient and low-carbon heating and cooling mechanisms can play a crucial role in addressing the rising demand for energy. Technologies such as solar-thermal, combined heat and power (CHP), heat pumps and thermal energy storage systems can reduce emissions and oil consumption [1]. In particular, the use of thermal energy storage technologies allow higher flexibility by minimizing energy production at partial loads or sub-optimal conditions, and shifting the energy demand over time to reduce the impact of peak loads. It also mitigates the need for expensive electrochemical energy storage. Similarly, the combination of thermal energy storage and CHP can reduce the transmission and distribution losses and improve the reliability of energy supplies. Thermal energy storage can facilitate a greater use of renewable energy such as solar radiation, with the additional capability to store thermal energy from waste heat sources over the course of hours to months. Consequently, cost reductions and improved performance are expected with low-cost thermal energy storage, which will allow active solar thermal systems to play an important role in realizing sustainable energy use.

Thermal energy storage has typically been carried out using thermophysical, thermochemical or a combination of these mechanisms. The characteristic energy densities for these approaches, however, are different. While the energy densities using thermophysical mechanisms such as sensible-heat [5] and latent-heat [6–9] are generally low, thermochemical energy storage by way of chemical reactions can provide significantly higher energy densities [5,10]. Sorption-based energy storage, involving the interaction of a gaseous adsorbate with a condensed medium, can either be thermophysical (e.g., physisorption) or thermochemical (e.g., chemisorption) [11]. Consequently, sorption can provide a wide range of energy densities with significantly lower heat losses, superseding the performance of typical energy storage techniques based on sensible-heat and latent-heat [10]. While chemisorption can achieve high specific energy (O(MJ/kg)) [12], several practical limitations [13,14] can impose challenges for its use in climate control systems. On the other hand, while physisorption may offer relatively lower energy densities, it is more easily incorporated in sorption-based heat pumps and can take advantage of a wider range of heat sources including solar energy.

For climate control, physisorption has been leveraged extensively in sorption-based heat pumps, which are designed to operate cyclically with a continuous heat input [15–37]. However, suffering from design and operational complexities, poor heat and mass transfer, and low power densities, sorption heat pumps have not gained wide acceptance. Therefore, more recent efforts have focused on new sorption materials [32,38,39], additives to enhance thermal transport properties [40,41], modified operational cycles [42] and innovative component designs [43] that can enhance the overall power densities for heating and cooling. Although some of the benefits of sorption-based climate control systems have been recognized, they have remained bulky and heavy, and the characteristic energy and power densities have remained relatively low, limiting wider implementation of sorption for energy storage in many applications.

In this work, we present the concept of a "thermophysical battery" based on physisorption, which can deliver both heating and cooling by storing energy (Fig. 1). It is designed to store and deliver thermal energy at relatively high power densities by identifying high-capacity sorption-pairs, and optimizing its design based on the choice of materials and operating conditions. Like a rechargeable electric battery, the thermophysical battery operates via charging and discharging mechanisms, and consists of two terminals, which in this case are the hot and cold terminals. The terminals are specifically designed to promote thermal transport, ensuring compactness and extraction of maximum power. The thermophysical battery can function with intermittent sources of heat and temporally-varying operating conditions.

Fig. 2 shows a comparison of thermophysical battery performance with commercial climate control systems based on vapor compression cycle (VCC), absorption (ABS) and adsorption (ADS) mechanisms. The power density and specific power for the thermophysical battery were obtained by normalizing the experimentally-demonstrated heating and cooling power with the total volume and mass of various components incorporated in the terminals of the battery, respectively. Since the choice of auxiliary components such as heat exchangers, pumps, fans, valves and piping can vary significantly with the application, they were not included in the calculation of power densities and specific powers shown in Fig. 2. While the current study incorporates contemporary materials for experimental characterization, with the inclusion of novel materials [44,45] and use of optimized and compact designs, the power density and specific power can be enhanced further (Fig. 2). This is particularly important for mobile applications such as temperature control for vehicles and storage and transportation of perishable cargo.

In the following sections, we elucidate several interesting aspects of the thermophysical battery, including the analogies to conventional electrochemical battery. In Section 2, we describe the working principle, design and operation of the thermophysical battery. In Section 3, we describe the experiments and computational model to characterize the overall performance. Section 4 discusses the performance results based on experiments and computational simulations. Section 5 provides the cyclic performance with different operational schemes, and Section 6 describes the future potential of the thermophysical battery.

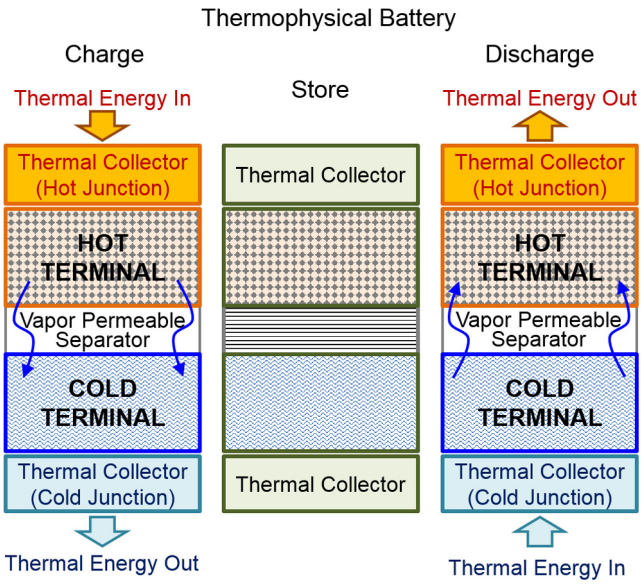

Fig. 1. A thermophysical battery consisting of hot and cold terminals designed to facilitate thermal energy storage and on-demand release for climate control.

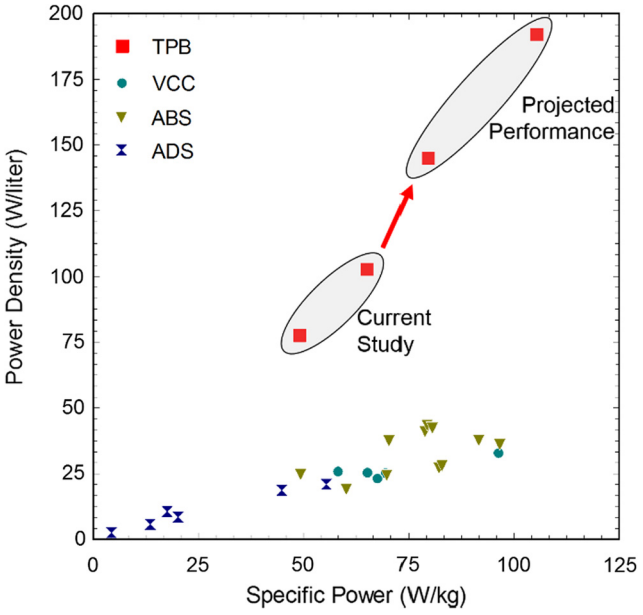

Fig. 2. Cooling and heating performance of the thermophysical battery (TPB) compared to the commercially-available climate control systems based on vapor compression cycle (VCC), absorption (ABS) and adsorption (ADS) mechanisms. Power density and specific power of the TPB were calculated by normalizing its performance with total mass and volume of materials incorporated in the hot and cold terminals of the TPB (auxiliary components like external heat exchangers, pumps, and piping were not considered). Projected performance of TPB was calculated based on the use of novel materials and design improvements. Power density and specific power of the commercial units were calculated using data on overall performance, mass and volume for various systems (auxiliary components were not included). More details are provided in supplementary information.

2. Thermophysical battery for climate control

The thermophysical battery is designed to store or release heat. Analogous to its electrochemical counterpart, it is operated with charging and discharging mechanisms. However, unlike an electrochemical battery where the flow of electrons takes place in an external circuit, the thermophysical battery enables thermal transport. The underlying physical mechanisms for heat extraction and generation are evaporation and adsorption, respectively, as opposed to electrochemical reactions. These processes take place in two different compartments or terminals, which are thermally isolated to maintain significantly different temperatures or thermal potentials (Fig. 3). As evaporation is endothermic and adsorption is exothermic, the corresponding compartments represent the cold (low thermal potential) and hot (high thermal potential) terminals of the thermophysical battery, respectively. The following sections describe the design, operation and performance characterization.

2.1. Working principle of a thermophysical battery

The terminals capable of providing a "thermal potential difference" are labeled as the adsorption bed unit (ABU) and the evaporator-condenser unit (ECU) (Fig. 3). The ABU, facilitating adsorption (discharge) and desorption (recharge) processes, is the hot terminal. The ECU, facilitating evaporation (discharge) and condensation (recharge) processes, is the cold terminal. The cyclic operation, involving the charging and discharging processes, is carried out by allowing directional flow of vapor molecules between the ABU and ECU, analogous to the transport of ions between the anode and cathode in an electrochemical battery.

A fully-charged thermophysical battery with the ABU and ECU initially at thermodynamic states 1 and 3, respectively, is discharged by allowing the transport of vapor from the ECU to the ABU (Fig. 3). During discharge, heat is supplied to the ECU matching the enthalpy of evaporation, and heat is released at the ABU matching the enthalpy of adsorption. Consequently, the ABU and ECU undergo transitions from states 1 to 2, and 3 to 4, respectively. This transition is facilitated by vapor transport driven by a concentration gradient, allowing molecules to migrate from the vapor-rich ECU to the vapor-deficient ABU. In order to sustain this process, the ABU is designed to provide a high vapor storage capacity. With both evaporation and adsorption processes taking place, vapor transport is sustained while the concentration gradient is maintained. However, the vapor transport will cease and the thermal potential difference will reduce once the thermophysical battery is discharged completely. This corresponds to a vapor-saturated ABU (state 2), and a depleted ECU (state 4).

The thermophysical battery is recharged by providing the heat of desorption at the ABU, which results in vapor desorption and its transport back to the ECU. The vapor entering the ECU condenses by releasing the heat of condensation. Consequently, during recharge, the ABU and ECU undergo transitions from states 2 to 1, and 4 to 3, respectively. The process is carried out until the ABU is evacuated and the ECU is replenished, restoring the initial conditions.

The working principle allows the thermophysical battery to maintain its terminals at different thermal potentials during discharge, providing a storage-based alternative for climate control. A wide range of heat sources can be used for recharge, including solar radiation, geothermal energy, combustion heat from coal or natural gas, and exhaust or waste-heat from industries and automobiles. As a result, direct utilization of thermal energy eliminates the inefficiencies associated with the use of electrically-driven heat pumps, which pay significant penalty for the generation [46] and distribution of electricity [47]. Like electrochemical batteries, the performance of the thermophysical battery relies on the choice of materials for energy storage. Furthermore, the performance quantified by the heating and cooling powers, depends on the thermal transport characteristics. The following sections describe the design to maximize thermal transport and energy storage.

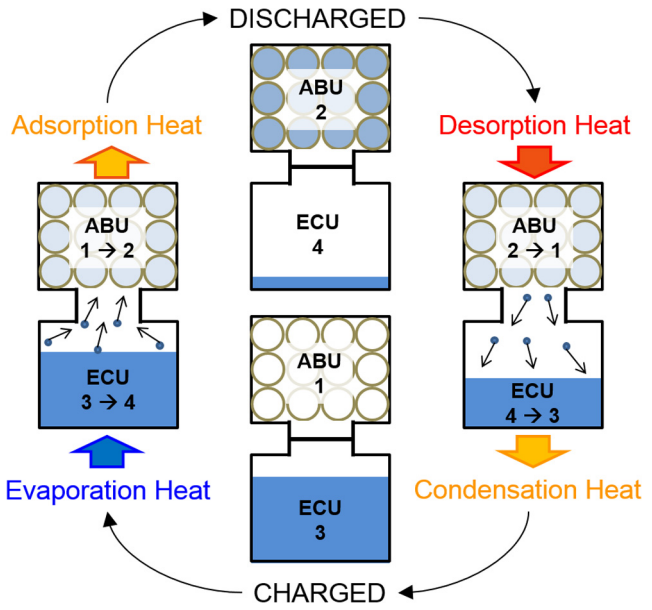

Fig. 3. The thermophysical battery is operated by cycling the ABU between the thermodynamic states 1 and 2, and the ECU between states 3 and 4. A fully-charged thermophysical battery consists of a dry ABU at thermodynamic state 1 and a refrigerant-filled ECU at state 3. Battery discharge takes place with the ABU undergoing adsorption, and the ECU undergoing evaporation, until the ABU is saturated with the refrigerant at state 2, and the ECU is empty at state 4. The battery is recharged by providing thermal energy or heat to ABU resulting in vapor desorption. The heat generated due to condensation in ECU during recharge can be rejected to the ambient. As a result, the ABU and ECU transition back from thermodynamic states 2 and 4 to 1 and 3, respectively, concluding the recharge process.

2.2. Design and operation of the thermophysical battery

To facilitate heating or cooling of an enclosed space, the thermophysical battery is interfaced with the enclosure and the ambient via heat exchangers or heat sinks (Fig. 4(a)). With the working principle described above, the enclosure can be cooled by interfacing it with the ECU, which allows heat extraction for the evaporation of the refrigerant. Alternately, the enclosure can be heated by interfacing it with the ABU, wherein the heat of adsorption can be utilized. After discharge, the thermophysical battery is recharged by supplying heat to the ABU (Fig. 4(b)). During recharge, the vapor desorbed from the ABU is condensed and collected in the ECU by rejecting the heat of condensation to the ambient.

The interfaces connecting the ABU and ECU with the enclosure and the ambient represent the external thermal circuit. In this regard, it is important to elucidate the role of two distinct fluids, the "refrigerant" and the "coolant", which serve different functions in the thermophysical battery. The refrigerant undergoes evaporation/condensation in the ECU, and adsorption/desorption in the ABU. On the other hand, the coolant is simply a carrier of thermal energy, which facilitates thermal transport between various components of the system. In other words, the transport of the vaporized refrigerant between the terminals of the thermophysical battery is analogous to the flow of ions in an electrochemical battery, and the coolant flow transferring thermal energy is analogous to the flow of electrons in the external circuit of the electrochemical battery. Both the ABU and ECU have dedicated coolant lines or thermal collectors (Fig. 4(c)). When the thermophysical battery is being discharged, heat is transferred from the coolant to the evaporating refrigerant in the ECU, resulting in a decrease in the temperature of the coolant exiting the ECU. On the other hand, due to vapor adsorption in the ABU, heat is gained by the coolant. Consequently, the temperature of the coolant exiting the ABU is higher. For recharging, while the ABU can be heated using various means, in this study it is carried out either by the electric heaters closely coupled with the ABU or by flowing a coolant at high temperature through the ABU.

Both ABU and ECU are designed to maximize vapor and thermal transport and minimize overall volume. The ECU is constructed to operate as an evaporator and condenser. In the current implementation, it simply consists of two helical coolant lines connected in series and placed at different elevations within the ECU. The lower helical line is submerged in the refrigerant pool while the upper helical line is located in the vapor space. The submerged coolant line is responsible for generating vapor during discharge, and the elevated coolant line allows condensation of vapor during recharge.

The ABU is designed to operate favorably during both the adsorption (discharge) and desorption (recharge) processes. The detailed design of the ABU with characteristic dimensions of the sub-components is shown in Fig. 4(d). The ABU was constructed using the contemporary adsorptive material NaX-zeolite. To promote vapor and thermal transport, the ABU consists of uniformly-spaced thin "adsorbent stacks" (≈2 mm), which are interfaced with the coolant lines. The small spacing between consecutive stacks minimizes the ABU volume while allowing vapor transport. The thickness and the density of the stacks were carefully chosen to provide maximum energy density while ensuring unimpeded vapor and thermal transport across the stacks [48]. A single stack of the ABU consists of two adsorption layers closely interfaced on both sides of an aluminum fin. Each adsorbent layer is a composite structure made by infusing NaX zeolite into porous (porosity >0.9) copper foam. This minimizes resistance to thermal transport across the adsorption layer, and maximizes heat conduction from the adsorbent to the aluminum fin. With this design, the heat generated by the adsorbent is conducted across the adsorption layer to the aluminum fin, and then to the coolant lines made from thin-walled copper tubing. The ABU stacks measure 160 mm × 80 mm × 4 mm, with each stack containing eight cavities of 10 mm diameter to interface with the coolant lines.

3. Performance characterization of thermophysical battery

A test bed was fabricated to demonstrate the operation of the thermophysical battery and quantify its overall performance (Fig. 5). The direction of coolant flow is marked by the arrows. To demonstrate the concept, while the ABU was constructed using NaX zeolite, the ECU was filled with deionized and deaerated water as the refrigerant. The coolant or thermal carrier for this study was water. Other options for a thermal carrier are ethylene glycol or a mixture of water and ethylene glycol, which can operate over a larger temperature range without undergoing phase change. Additional information regarding the test bed and fabrication process is provided in supplementary information. The ABU and ECU constructed for performance quantification are shown in Fig. 6.

3.1. Experimental characterization of battery operation

For experimental characterization, the ECU was connected to a temperature controller to receive coolant at a constant temperature and the ABU was interfaced with an air heat exchanger to facilitate heat transfer to the ambient. Starting with a fully-charged thermophysical battery, the change in the thermal potentials at the terminals was monitored in the experiments. The coolant lines connected to the ABU and ECU were interfaced with temperature sensors (Fig. 5) to quantify the total heat flow rate, $\dot{Q}$. The total heating and cooling powers can be calculated using the coolant temperatures and flow rate.

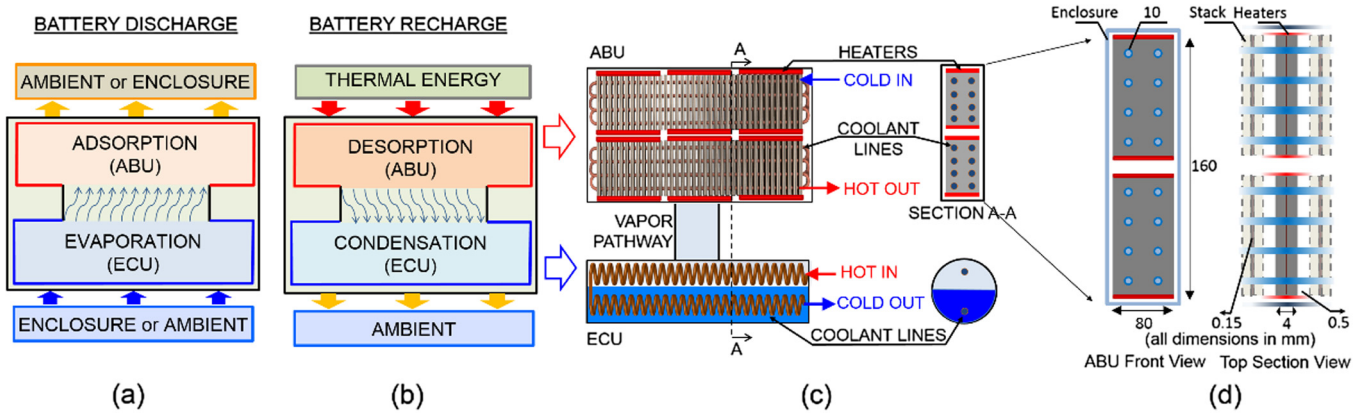

Fig. 4. (a) During discharge heat is absorbed in the ECU for evaporation and generated in the ABU due to adsorption. (b) During recharge heat is supplied to the ABU causing desorption and heat is rejected in the ECU due to vapor condensation. (c) The ABU consists of multiple rows of "adsorbent stacks" interfaced with coolant lines and heaters, while the ECU consists of helical tubing to facilitate coolant flow and evaporation/condensation processes. Cross-sectional views (section A-A) show details of the ABU and ECU geometry. (d) Detailed geometric characteristics of ABU sub-components are shown.

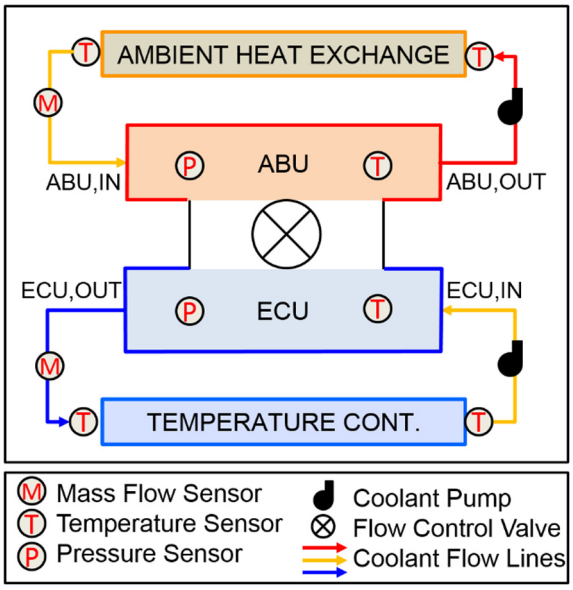

Fig. 5. The experimental test bed constructed to demonstrate the concept of the thermophysical battery. It incorporates several temperature (T), pressure (P) and flow sensors (M) to study the overall performance. Apart from the ABU and ECU, a recirculating heater was used as a temperature controller to provide coolant at desired temperature to the ECU and an air-heat exchanger was used to dissipate heat generated in the ABU to the ambient.

$$\dot{Q}_{ABU} = \rho_c \dot{V}_{ABU} c_{pc} (T_{ABU,OUT} - T_{ABU,IN}) \quad (1)$$

$$\dot{Q}_{ECU} = \rho_c \dot{V}_{ECU} c_{pc} (T_{ECU,OUT} - T_{ECU,IN}) \quad (2)$$

Here ρ_c and c_{pc} are the density and specific heat capacity of the coolant, respectively, and $\dot{V}$ is the volumetric flow rate of the coolant. Using the pressure and temperature sensors embedded in the ABU and ECU, the average concentration of the vapor can be determined using the ideal gas law as,

$$\rho_{V,ABU} = p_{ABU}/R_g T_{ABU} \quad (3)$$

$$\rho_{V,ECU} = p_{ECU}/R_g T_{ECU} \quad (4)$$

Using the propagation of uncertainty [49], the errors in the measurement of volumetric flow rate, temperature and pressure were used to calculate the uncertainties in the heating and cooling powers and the vapor densities. Details regarding the uncertainty analysis are provided in supplementary information. In addition to the demonstration of the concept, it is useful to study the effect of several operational parameters on system performance, which was carried out by a computational analysis, as discussed below.

3.2. Computational study of battery operation

The overall performance depends on the adsorption dynamics in the ABU and evaporation in the ECU, which can be estimated by studying the representative unit cells of the ABU and ECU

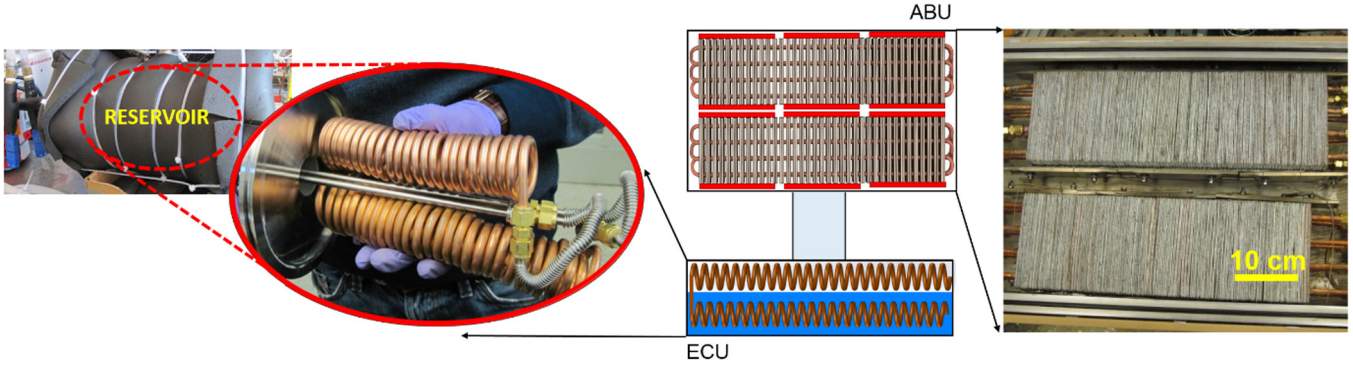

Fig. 6. The interior structures of ECU (left) and ABU (right) are shown. The ABU shown with the enclosure ceiling opened, is constructed as two blocks, with each block interfaced with heaters for battery recharge. Each block consists of ~100 adsorption stacks, each of which is interfaced with eight coolant lines. The ECU is shown consisting of two sets of helical coils, each utilized either for condensation (during recharge) or evaporation (during discharge) process.

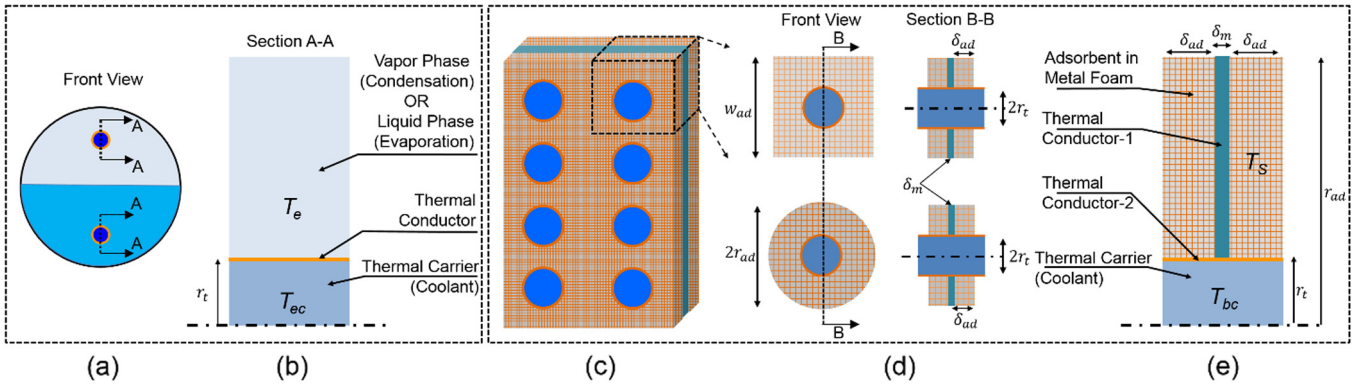

Fig. 7. The computational analysis of evaporation in the ECU (a) is carried out by considering its representative unit cell (b), and the analysis of adsorption in ABU stack (c) is carried out by considering an equivalent cylindrical geometry (d), which can be simplified as an axisymmetric geometry (e). Geometric parameters indicated in the figure are provided in supplementary information.

(Fig. 7). In the following sections, we describe the equations governing the performance of the battery.

3.2.1. Vapor and thermal transport in the ABU

The square-shaped unit cell of the ABU stack used in this study is approximated with an axisymmetric geometry (Fig. 7) by conserving the total mass of adsorbent per unit cell. This captures the multidimensional nature of transport during adsorption within the stack more accurately. The characteristic dimensions of the unit cell (Fig. 7) are provided in supplementary information. Vapor transport in the stack is analyzed using the following equation [48]

$$\varepsilon_s \frac{\partial C_s}{\partial t} = \varepsilon_s \nabla \cdot (D_s \nabla C_s) - \dot{C}_s \tag{5}$$

where C_s is the local vapor concentration, and $\dot{C}_s$ is the local adsorption rate in the stack. ε_s is the porosity and D_s is the vapor diffusivity for intercrystalline diffusion between adsorbent crystals (see inset in Fig. 8). $\dot{C}_s$ is calculated using the linear driving force model [50], to determine the adsorption rate within a single adsorbent crystal. Accounting for the packing density of the adsorbent, $\dot{C}_s$ is predicted using the adsorption rate within a single crystal,

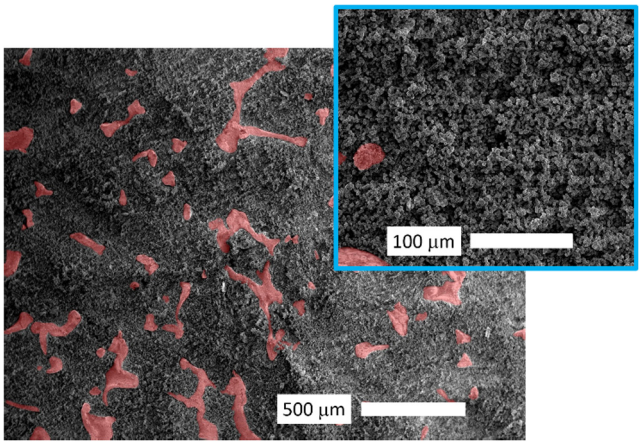

Fig. 8. Scanning electronic microscope (SEM) image of NaX-zeolite infused into porous (>0.9) copper foam. The copper foam holds zeolite and enhances the thermal conductivity for heat transfer. The inset shows high-magnification SEM indicating intercrystalline voids that allow vapor transport via diffusion. The SEM images are artificially colored to differentiate zeolite (grey) from copper (red). (For interpretation of the references to color in this figure legend, the reader is referred to the web version of this article.)

$$\dot{C}_s = 15(1-\varepsilon_s) D_c (C_{eq} - C_c)/r_c^2 \tag{6}$$

Here D_c represents the diffusivity of vapor inside a crystal (intracrystalline) of an equivalent radius r_c, characterized using a vapor sorption analyzer (supplementary information). C_c is the average concentration of adsorbed vapor in the crystal, and C_{eq} is the equilibrium concentration of adsorbed vapor corresponding to the local temperature, T, and pressure, p, surrounding the crystal. C_{eq} can be obtained from the adsorption isotherm for a given adsorbent-refrigerant pair. For this study, which incorporates the zeolite NaX-water pair, the Dubinin–Radushkevich equation [51,52] is used.

$$C_{eq} = C_{eq}^{o} \exp\left\{ -\left[\frac{\hat{R}T}{\beta E_o} \ln\left(\frac{p_{sat}}{p} \right) \right]^2 \right\} \tag{7}$$

Here C_{eq}^{o} is the maximum adsorption capacity, E_o is the characteristic adsorption energy and β is an isotherm constant called the affinity coefficient. The vapor uptake or the mass of vapor adsorbed per unit mass of adsorbent is given as $\omega = C_{eq} M/\rho_{ad}$, where M is the molar mass of the refrigerant and ρ_{ad} is the dry density of the adsorbent. The adsorption isotherm is characterized via thermogravimetric analysis, as described in supplementary information.

Assuming local thermal equilibrium between the adsorbent and the vapor, the spatiotemporal variation in the stack temperature, T_s, is calculated using the following equation. Here convection is neglected compared to diffusion. Note that this is not generally the case since adsorbents are typically poor thermal conductors. However, when the adsorbents are packed in thermally-conductivity porous materials, such as metallic or graphitic foams, this assumption is valid. In this study, NaX zeolite is infused into a highly porous copper foam matrix (Fig. 8). Stack-level thermal transport is approximated as

$$\rho_s c_{ps} \frac{\partial T_s}{\partial t} = \nabla \cdot k_s \nabla T_s + \dot{C}_s h_{ad} \tag{8}$$

Here $\rho_s c_{ps}$ and k_s denote the average heat capacity and thermal conductivity, respectively. $\dot{C}_s h_{ad}$ is the rate of heat generation, where h_{ad} is the heat of adsorption. While the analysis of a unit cell considers rate limitations within the stack, the transport across the ABU also encounters bulk diffusion and advection resistances. Consequently, these transport resistances can further delay adsorption kinetics. For simplicity, the current study neglects these resistances in comparison to transport limitations within a stack, which are expected to be much higher.

Taking into account the void volume in the ABU, the total adsorption rate in the ABU, $\dot{C}_b$, is calculated as follows.

$$\dot{C}_b = \int \dot{C}_s dV_{ABU} \tag{9}$$

Note that the computational model is applicable for analyzing both recharge and discharge processes, wherein $\dot{C}_b$ represents the rate of adsorption or desorption.

In addition to the governing equations mentioned above, initial and boundary conditions are necessary for the prediction of vapor and thermal transport in the stacks. The ABU is initially at temperature, $T_{s,i}$, and vapor pressure, p_i, which corresponds to an adsorbed phase equilibrium concentration, $C_{eq,i}$. The stacks are then exposed to vapor, where either the vapor pressure in the ABU, p_b, or vapor flux supplied from the ECU, $\dot{C}_b$, is known, which results in adsorption and heat generation in the ABU. Both p_b and $\dot{C}_b$ are experimentally-controllable parameters. The heat generated in the stacks during adsorption is carried away by the coolant in the thermal circuit whose temperature, T_{bc}, is known and the overall thermal conductance, $(UA)_b$, is evaluated using the existing correlations for heat transfer coefficient [53]. Therefore, the instantaneous rate of heat released from the ABU to the coolant is given by

$$\dot{Q}_{ABU} = (UA)_b (T_s - T_{bc})_{LM} \tag{10}$$

$(T_s - T_{bc})_{LM}$ is the characteristic (log-mean) temperature difference between the ABU and the coolant, given by

$$(T_s - T_{bc})_{LM} = \frac{(T_{bc,o} - T_{bc,i})}{\ln[(T_s - T_{bc,o})/(T_s - T_{bc,i})]} \tag{11}$$

where $T_{bc,i}$ and $T_{bc,o}$ denote the inlet and outlet temperatures of the coolant flowing through the ABU, respectively. In order to quantify the temporal variation in temperature and pressure of the ABU via computational analysis, these variables are spatially averaged using stack volume, V_s.

$$T_{ABU} = \int T_s dV_s / V_s \tag{12}$$

$$p_{ABU} = \int C_s \hat{R} T_s dV_s / V_s \tag{13}$$

Additionally, the extent of adsorbent use over time is determined by the spatially averaged net vapor uptake,

$$\bar{\omega} = \int (\omega dV_s)/V_s \tag{14}$$

3.2.2. Phase-change and transport in the ECU

Analysis of evaporation and thermal transport in ECU is carried out by considering a representative unit cell (Fig. 7) wherein the geometric parameters and thermophysical properties relevant to the ECU are provided in supplementary information. During discharge, the helical tubes of the evaporator submerged in a pool of liquid facilitates evaporation of the surrounding liquid. On the other hand, during recharge, the helical tubes surrounded by vapor cause condensation. Since evaporation and condensation processes in the ECU are induced by vapor adsorption and desorption processes in the ABU, respectively, the analysis of vapor transport in the ECU is carried out knowing the total rate of adsorption or desorption in the ABU. Assuming that phase change in the ECU is not rate limiting compared to adsorption dynamics in the ABU, the vapor transport limitations and temperature gradients within the ECU are neglected. The temporal variation in the temperature of the ECU, T_e, is then calculated using the following equation,

$$\rho_e c_{pe} \frac{dT_e}{dt} = \dot{Q}_{eV} + \dot{Q}_{ec} \tag{15}$$

where $\dot{Q}_{eV}$ is the heat generation or absorption rate and $\dot{Q}_{ec}$ is the heat exchanged with the coolant flowing across the ECU. Volumetric integration of the equation results in the following,

$$m_e c_{pe} \frac{dT_e}{dt} = \dot{C}_b h_{eV} + (UA)_e (T_{ec} - T_e)_{LM} \tag{16}$$

where $m_e c_{pe}$ is the time-varying total heat capacity of the ECU, which includes the capacitance due to the refrigerant and metallic components such as the coolant lines, $(UA)_e$ is the overall heat conductance of the thermal circuit interfaced with the ECU evaluated using existing correlations for heat transfer coefficient [53], and T_{ec} is the temperature of the coolant in the circuit. The instantaneous heat supplied by the ECU to the coolant during evaporation or condensation is calculated using the following equation,

$$\dot{Q}_{ECU} = (UA)_e (T_e - T_{ec})_{LM} \tag{17}$$

$(T_e - T_{ec})_{LM}$ is the log-mean temperature difference between the ECU and the coolant, given by

$$(T_e - T_{ec})_{LM} = \frac{(T_{ec,i} - T_{ec,o})}{\ln[(T_{ec,i} - T_e)/(T_{ec,o} - T_e)]} \tag{18}$$

where $T_{ec,i}$ and $T_{ec,o}$ denote the inlet and outlet temperatures of the coolant flowing through the ECU, respectively. Like the ABU, initial conditions are necessary for estimating the ECU performance. Initially, the ECU is assumed to be in thermal equilibrium with the coolant and at saturation conditions corresponding to the coolant temperature, T_{ec}.

Eqs. (5)–(18) are utilized for performance prediction at different operating conditions, which are listed in supplementary information.

4. Results and discussion

The following sections describe the overall performance using experiments and computational analysis. While the experiments demonstrate the feasibility of this technology, they also identify factors controlling the overall performance. The computational analysis for predicting the performance of the thermophysical battery is compared with the experiments to show good agreement. Subsequently, the computational model is used to gain further understanding and predict performance during cyclic operation.

4.1. Vapor transport between ABU and ECU

A flow control valve (Fig. 5) is used to connect the ABU and ECU, which can be closed completely to isolate the terminals of the thermophysical battery. However, once the valve is opened, vapor flow is automatically initiated from the ECU to the ABU. Therefore, in this context, the valve can be considered as a variable resistor controlling vapor flow, to extract desirable power. For the current implementation, it is important to determine factors driving vapor transport.

Fig. 9(a) and (b) shows the variations in the vapor pressure and vapor density (Eqs. (3) and (4)), respectively, in the ABU and the ECU as a function of time. The initial difference in vapor pressure between the two terminals is evident, wherein both the ABU and ECU are in thermal equilibrium with the ambient and the valve is closed, blocking vapor transport completely. Initially the pressure in the ABU is negligibly small, and the ECU is at the saturation pressure of the refrigerant (water) corresponding to the coolant temperature. Once the battery discharge is initiated with the opening of the valve, the vapor phase experiences a large pressure gradient in the first forty minutes of operation (Fig. 9(a)). Consequently, the vapor molecules experience significant acceler-

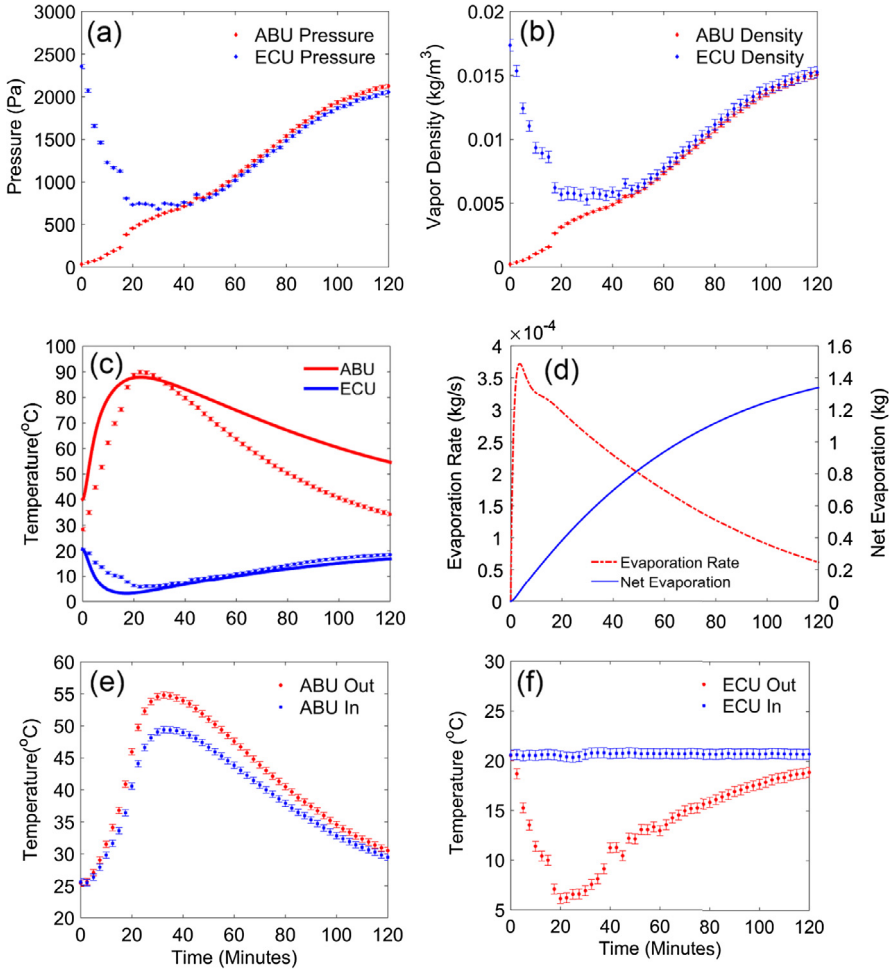

Fig. 9. Temporal variation in (a) vapor pressure and (b) vapor density in the ABU and ECU, (c) thermal potential at the terminals (discrete points are from the experiments and continuous lines are from the computational study), (d) rate of evaporation and net evaporation obtained from computational analysis, and inlet/outlet temperatures of the coolant streams passing through the ABU (e) and ECU (f).

ation while undergoing expansion during their transit from the ECU to ABU. The pressure gradient between the terminals gradually decreases to become relatively small. Yet, vapor transport is sustained with evaporation and adsorption processes continuing to take place in the ECU and ABU, respectively. This is possible due to the presence of a vapor density gradient (Fig. 9(b)), which allows transport to continue via diffusion. In contrast, during recharge it is expected that the vapor in the ABU will correspond to a higher density compared to that in the ECU. Therefore, vapor density gradient is important for sustaining vapor transport in both directions. This indicates another important requirement to ensure successful operation and extract maximum power – it is essential to minimize the presence of any non-condensable molecules in the battery. Non-condensable molecules can significantly decrease vapor diffusivity, D_s, which will reduce vapor transport to adversely affect the overall performance of the thermophysical battery. The procedure used to remove non-condensable molecules from the system is described in supplementary information.

4.2. Thermal potentials of ABU and ECU

The changes in thermal potentials of the ABU and ECU with time are obtained through experiments and computational analysis (Fig. 9(c)). During discharge, the vapor is pulled away from the ECU causing evaporation. Since the process is endothermic, the ECU sustains evaporation with reduction in internal energy, which results in a significant decrease in the ECU temperature. On the other hand, vapor entering the ABU undergoes adsorption, resulting in the release of energy, a large portion of which increases the internal energy, and as a result the temperature of the ABU. The thermal potential difference continues to rise while the internal energies of the terminals change to support evaporation and adsorption processes. However, once the rate of energy exchanged with the coolant lines becomes as significant as the rate of change in the internal energies, the difference in thermal potentials will stop increasing and subsequently show a decreasing trend, which was captured by the experiments and the computational model. The potential difference increases in the initial twenty minutes of operation, reaching a maximum difference of 85 °C. Subsequently, there is a gradual drop in the potential difference, due to the equalizing effect of the heat exchanged between the coolant lines and the ABU and ECU, eventually returning them to the state of equilibrium or complete discharge. While the computational predictions are generally in good agreement with the experiment, the difference is mainly due to the omission of thermal losses and inter-stack transport resistances in the computational analysis. In addition, the computational analysis assumes thermal equilibrium between the vapor and solid phases. These approximations and neglecting the thermal gradients in vapor and solid phases make the model predictions ideal compared to experiments. As a result, it can be seen that the temporal variation in the predicted temperature difference is marginally faster and higher than the experiments.

The decrease in the thermal potential difference after twenty minutes of operation is not due to the cessation of adsorption and evaporation. In fact, these processes continue to take place, as indicated by the computational analysis, which predicts the evaporation rate as a function of time (Fig. 9(d)). Since vapor accumulation between the terminals is negligible, the net evaporation rate also represents the net adsorption rate. The initial adsorption rate is low due to low vapor pressure or concentration in the ABU. However, as the pressure in the ABU increases, there is a steep rise in the adsorption rate, reaching a maximum value which is controlled by the resistance to vapor transport between the terminals. After twenty minutes of operation, while the thermal potential difference has already reached a maximum value and starts decreasing, adsorption continues at a significant rate (Fig. 9(d)). Therefore, the decrease in the thermal potential difference is due to the combination of decreasing rate of heat generation and continuous heat exchange with the coolant lines. Additionally, since substantial mass transfer takes place between the two terminals (Fig. 9(d)), the temperature variation is also affected by the variation in the thermal capacitance of the ABU and the ECU.

4.3. Thermal transport in the coolant lines or thermal circuits

As mentioned before, the performance is experimentally characterized by interfacing the ABU with an air heat-exchanger to facilitate heat transfer from the ABU to the ambient air, and the ECU is interfaced with a temperature controller which supplies coolant at a desired temperature and flow rate. Consequently, the temperature profiles of the coolant entering each terminal are different (Fig. 9(e) and (f)).

Due to the heat released during adsorption, the coolant at the outlet is significantly warmer than the inlet of the ABU. Similarly, since heat is absorbed for evaporation, the coolant exiting the ECU is significantly colder than the inlet. The deviation of the coolant temperatures from the ambient temperature can be maintained for a significant duration, allowing heat exchange, which demonstrates the feasibility of this strategy for climate control. For instance, in this case, while the ambient temperature is 20 °C, the coolant exiting the ABU can continue to supply heat at temperatures exceeding 40 °C, and the coolant exiting the ECU can absorb heat at temperatures under 15 °C for more than sixty minutes. For both the ABU and ECU, the temperature change in the coolant from inlet to outlet increases from zero to a maximum value, followed by a gradual decrease back to zero. This temperature variation sustained during operation depends on two important factors, which are the rate of adsorption or evaporation, and the representative thermal conductance of each circuit. Consequently, the adsorbent-refrigerant pair and the coolant operating conditions can be chosen to control the heating and cooling powers to match the climate control demand.

4.4. Characterization of total heating and cooling power

The overall heating and cooling powers are measured in the experiments and predicted by the computational model (Fig. 10). The heating power is shown positive and cooling power is shown negative to signify the direction of heat transfer supplied by the thermophysical battery. With the current design and materials incorporated in the battery, significant power (≈1 kW) can be delivered for climate control. In this case, the temporally averaged heating power, which is delivered over 60 min at temperatures exceeding 40 °C, is more than 900 W. Similarly, the average cooling power, which is delivered for more than 60 min at temperatures under 15 °C, exceeds 650 W. The maximum heating and cooling powers observed were 1300 W and 980 W, respectively. While this was obtained using the NaX-water pair, it can be further enhanced

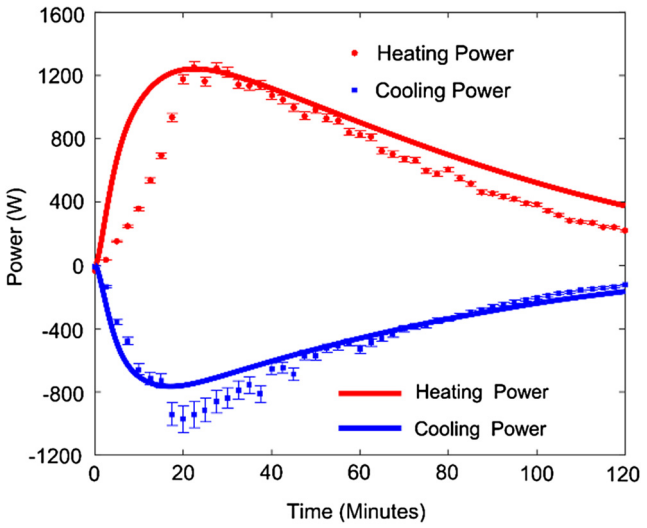

Fig. 10. The overall performance of the thermophysical battery is shown as a function of time with experimentally measured heating and cooling powers (discrete points) and computationally predicted heating and cooling powers (continuous line).

by incorporating adsorbents with higher adsorption capacities. Based on the total mass of adsorbent and vapor, the corresponding time-averaged material-level specific heating and cooling powers exceed 130 W/kg and 95 W/kg, respectively. Based on the total volume of adsorbent stacks (i.e., with the inclusion of intercrystalline porosity accounting for adsorbent packing density) the power densities for heating and cooling exceed 85 W/l and 60 W/l, respectively. The maximum power density and specific power observed, taking into account the total mass and volume of all subcomponents incorporated in the ABU and ECU, for both cooling and heating, are shown in Fig. 2.

Fig. 10 also shows that the heating and cooling powers are neither equal nor symmetric. This is expected since the adsorption energy, h_{ad}, is much higher than the evaporation energy, h_{eV}, both of which depend on the choice of adsorbent and refrigerant. There is also a large difference in thermal capacitance of the ABU and ECU. Consequently, the rates of energy produced or consumed at the two terminals are different. Apart from the ABU and ECU, the heating and cooling powers also depend on the temperature, overall conductance and capacitance of the thermal circuits interfaced with the ABU and ECU. The resulting asymmetry due to all the factors combined is captured in experiments and computational predictions.

An important aspect of the thermophysical battery operation is its temporally varying performance, which includes the thermal potential (Fig. 9(c)) and the power delivered (Fig. 10). As noted before, this is due to the chosen operating conditions for the experiments, wherein the vapor pressure in the ABU was allowed to increase linearly with time (Fig. 9(a)). Instead, it is possible to control the power output from the ABU and ECU by implementing a dynamically-controlled vapor flow mechanism. With the control of vapor flow, the total useful duration of discharge can be extended by delivering the required power for heating and cooling at the desired temperature. In this regard, the subsequent section quantifies the cyclic performance of the battery with the choice of operational strategy.

5. Cyclic performance of thermophysical battery

Apart from the choice of the adsorbent-refrigerant pair and the overall design of the sub-components, the cyclic performance also depends on the operating conditions. We focus mainly on the per-

formance of the ABU, which drives the process of phase-change and vapor transport in the thermophysical battery. Based on the mass of adsorbent incorporated in the current setup, a total heating capacity of 2 kWh is possible. In other words, with an average thermal power of 1 kW, the thermophysical battery can be discharged for a duration of 120 min.

As opposed to a linearly varying pressure (versus time), the most common technique is the implementation of the thermodynamic cycle for the sorption heat pump (Fig. 11(a)). The ABU is cycled between states A_1 and A_2 via constant pressure and constant vapor uptake processes. The ECU on the other hand is transitioned between states E_3 and E_4. With the overall operation based on this thermodynamic cycle, the temporal performance (Fig. 11(c)) is predicted using the computational model discussed above. The first half of the cycle indicates regeneration, wherein the ABU undergoes desorption for 120 min. This is carried out by supplying heat to the ABU from the coolant at 300 °C, while the ABU is maintained at a constant pressure of ~7400 Pa. The next half-cycle indicates discharge, wherein the ABU undergoes adsorption for 120 min. This is carried out by exposing the ABU to a constant vapor pressure of ~900 Pa, while maintaining the coolant flow through the ABU at a constant temperature of 40 °C. While the cycle is carried

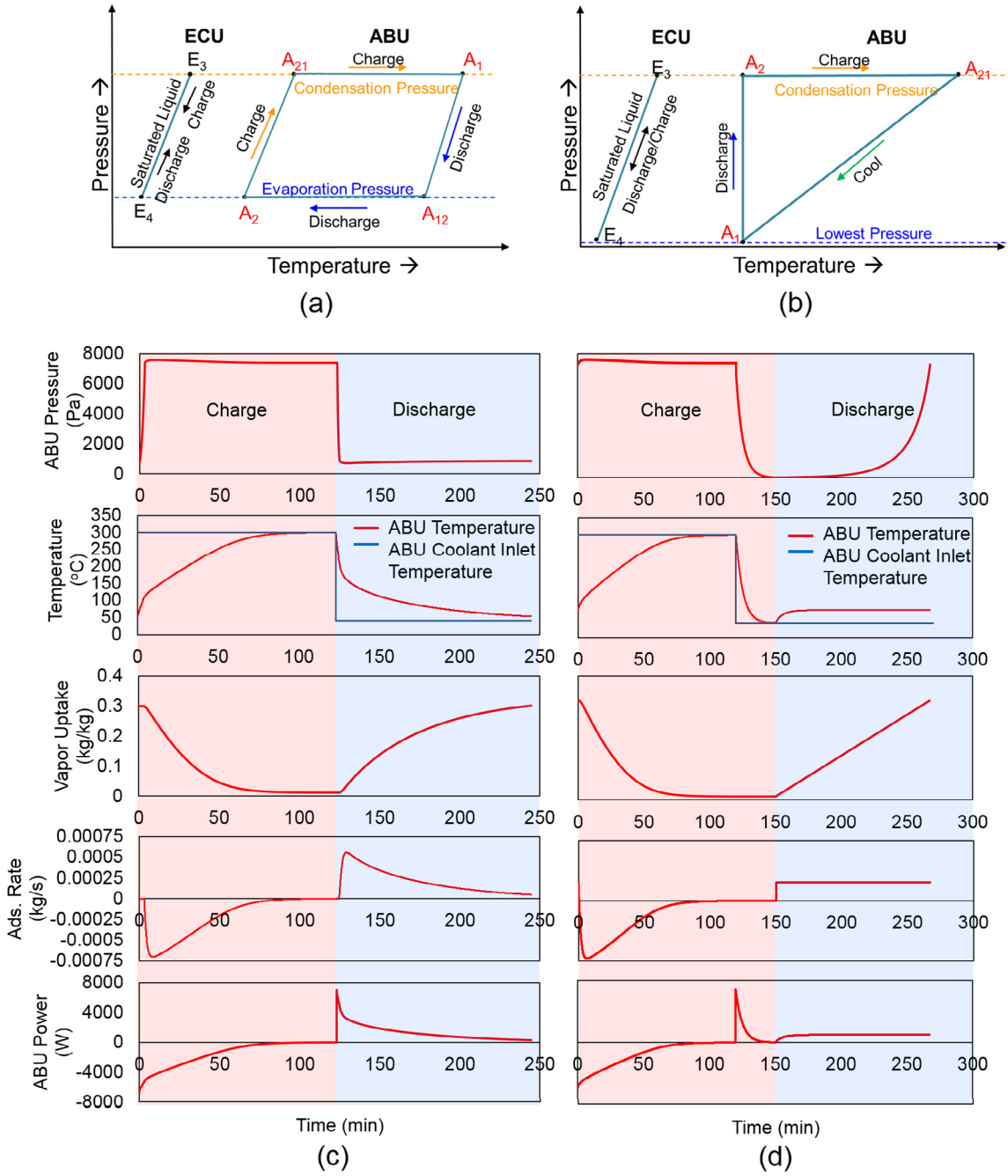

Fig. 11. The thermophysical battery can be operated cyclically following (a) conventional sorption heat pump cycle, or (b) consisting of an isobaric (A_2 to A_{21}), isosteric (A_{21} to A_1) and isothermal process (A_1 to A_2), wherein the charging and discharging processes are indicated by the arrows. Meanwhile, the ECU is transitioned between different pressures along the saturated liquid line between states E_3 and E_4. The cyclic performances corresponding to thermodynamic cycles in (a) and (b) are shown in (c) and (d), respectively.

out by fixing the pressures and coolant temperatures, the ABU temperature, vapor uptake, adsorption rate, and thermal power vary with time, as shown in Fig. 11(c).

During the charging process from 0 to 120 min, the ABU temperature is raised, resulting in desorption and a decrease in the net vapor uptake, which transforms the thermophysical battery from an initial thermodynamic state A_2, which corresponds to low temperature (40 °C) and high saturation ($\sim$0.3 $kg_{water}/kg_{adsorbent}$) to the final state A_1, which corresponds to high temperature (300 °C) and low saturation ($\sim$0 $kg_{water}/kg_{adsorbent}$). During the discharge process carried out from 120 to 240 min, the ABU temperature decreases and the net vapor uptake increases due to exposure to vapor, transforming it back from state A_1 to A_2.

During the transition between states A_1 and A_2, the variation in the adsorption rate and power is also shown in Fig. 11(c). Here negative values indicate vapor desorption and the delivery of heat to the ABU, and positive values indicate vapor adsorption and heat released from the ABU to the coolant. It is clear that by maintaining a constant vapor pressure in the ABU during adsorption and desorption, the overall performance is highly transient and a constant heating or cooling power cannot be achieved. The adsorption rate and discharge power attain a maximum value in the initial stages, followed by a steep decrease. While this operational scheme may be desirable for applications that require an initial surge in performance, it may not be suitable for applications desiring a constant power output.

As opposed to maintaining a constant pressure in the ABU, like contemporary sorption cycles, it is possible to control the mass flux entering the ABU with the use of the flow control valve. The thermophysical battery can be operated based on a new thermodynamic cycle (Fig. 11(b)), with a temporal performance shown in Fig. 11(d).

The thermophysical battery is recharged by providing heat to the ABU at a constant pressure, which transforms the ABU from a low-temperature saturated state-A_2 to a high-temperature dry state-A_{21}. As shown in the temporal performance, the recharge process is carried out for a duration of 120 min, where the ABU is exposed to vapor at $\sim$7400 Pa and coolant at 300 °C. The vapor leaving the ABU undergoes condensation in the ECU, which is maintained at state E_3. During the recharge process, the ABU temperature is increased gradually (Fig. 11(d)). As a result of the thermally driven desorption process, the vapor uptake is reduced from $\approx$0.3 $kg_{water}/kg_{adsorbent}$ to $\approx$0 $kg_{water}/kg_{adsorbent}$. Higher desorption rate and power during initial stages of recharge is due to the presence of a significant amount of adsorbed vapor in the ABU. Subsequently, the desorption rate and power diminish significantly.

Following the heating process, the ABU is isolated from the ECU by closing the flow control valve completely. In addition, the ABU is cooled down by transferring heat to the coolant at ambient temperature (40 °C), which transforms it from a high-temperature dry state-A_{21} to a low-temperature dry state-A_2 (Fig. 11(b)). In this case, the cooling process is carried out for 30 min, which brings the ABU back to the ambient temperature (Fig. 11(d)). Due to a lack of vapor supply from the ECU, the pressure inside the ABU reduces significantly due to re-adsorption of trace amounts of vapor surrounding the adsorbent material. The net energy rejected by the ABU to the coolant during the cool down process is predominantly sensible heat. The thermophysical battery can be stored at state A_1 for extended durations without loss in performance. Note that in comparison, it is significantly more challenging for conventional techniques (e.g., energy storage via phase change materials and sensible heat) to minimize loss in performance during storage.

The thermophysical battery is discharged when the valve between the ABU and ECU is opened and dynamically controlled, allowing evaporation and adsorption processes to take place at the desired rate. Consequently, the ABU is exposed to a constant vapor flux, transforming it from state A_1 to A_2 due to vapor adsorption (Fig. 11(d)). In this case, using the current test bed, the vapor flux chosen for operation can generate a constant heating rate of 1 kW at the ABU. In this process, both the ABU and the ECU are exposed to intermediate pressures that vary between the low pressure limit and the condensation pressure. Specifically, the pressure profile for constant vapor flux (Fig. 11 (d)) indicates that the ABU pressure does not change appreciably for a significant duration due to the continuous adsorption of vapor. However, once the adsorbent approaches saturation conditions, there is a rapid rise in pressure until the condensation pressure is reached. As expected due to a constant mass flux, the vapor uptake increases linearly with time. More importantly, it can be seen that the ABU generates and supplies heat at a constant rate to the coolant. This operating condition is reached within a few minutes of initiating discharge. In addition, by maintaining steady coolant flow conditions, the thermal potential of the ABU remains fixed during the discharge process. In this case, the thermal potential of the ABU is maintained at 80 °C, while the coolant is circulated at 40 °C. Of course, the steady thermal potential maintained in the ABU can also be altered by changing the coolant flow rate, which will change the overall thermal conductance of the coolant circuit.

While the thermophysical battery can be operated to provide a wide range of powers and thermal potentials, the overall duration of steady operation relies on the storage capacity of the adsorbent. Consequently, while the performance in this study was quantified using conventional adsorbents, such as zeolite NaX, we anticipate a significant increase in the energy and power density with the use of novel adsorbents and nanomaterials for enhanced thermal transport [38,39,44,45]. This will promote the development of a variety of systems for temperature control with a wide range of energy storage capacities, and heating and cooling powers. As a result, several applications such as climate control in buildings, temperature control in vehicles and other mobile systems, and storage of perishable goods and heat-sensitive materials can benefit from this technology.

6. Conclusions

Thermal energy storage-based climate control offers a promising strategy to address the rising demand for energy. While allowing higher flexibility in energy usage, it can facilitate greater use of renewable energy with the ability to store solar energy and waste heat for extended durations. The thermophysical battery, which operates using adsorption/desorption and evaporation/condensation mechanisms, can successfully deliver climate control on-demand by storing energy that can be captured from a wide range of heat sources. It consists of hot and cold terminals, which can be maintained at different thermal potentials. Based on the underlying mechanisms of adsorption-desorption and evaporation-condensation the hot and cold terminals are called the ABU and ECU, respectively. Like a conventional electrochemical battery, the thermophysical battery can operate cyclically via charging and discharging processes. It is designed to store and deliver high energy and power densities by leveraging high-capacity sorption-pairs and optimizing the performance based on the choice of materials and operating conditions. Unlike a traditional heat pump, it can be operated with intermittent heat sources to provide climate control.

Using NaX-water pair, this study demonstrates heating in excess of 900 W at temperatures exceeding 40 °C, and 650 W of cooling at temperatures less than 15 °C. The maximum heating and cooling powers observed were 1300 W and 980 W, respectively. This corresponds to power densities and specific powers of 103 W/l and 65 W/kg for heating, and 78 W/l and 49 W/kg for

cooling, respectively, making thermophysical battery competitive with the state-of-the-art climate control systems that provide lower power densities.

Temporal performance characterization indicates that the power and thermal potentials delivered at the terminals can vary significantly in time. Consequently, we show that it can be operated following different operational strategies, allowing the supply of heating or cooling power as desired by the application of this technology. While it is possible to provide an initial surge in performance, a steady performance with constant heating and cooling power and thermal potential is also realizable. These operational characteristics can be implemented with a simple flow control mechanism to modulate vapor transport between the ABU and the ECU.

While our initial study shows many interesting aspects related to the performance of the thermophysical battery, there are several opportunities for further study and development. While the current system utilizes NaX zeolite, the use of novel adsorbents such as metal-organic frameworks [45,54] and emerging zeolites [39] can enhance the overall performance of the battery significantly. The current design of the ABU is optimized for the use of NaX zeolite without densification. The design of ABU and ECU can be tailored and optimized to suit the integration of novel adsorbents along with compaction strategies, which can result in higher energy and power densities. This can be carried out by analyzing and quantifying adsorption characteristics, vapor and thermal transport at the material- and component-levels. On the system-level, the development of feedback control strategies can modulate the heating and cooling powers to meet the desired climate control demands and improve the overall efficiency of operation. While the current study demonstrates storage of thermal energy released by resistive heating, interfacing the thermophysical battery with other sources of energy such as waste heat from industries and vehicular exhaust, solar radiation, and geothermal energy will be very useful. With these improvements, the thermophysical battery can be made environmentally sustainable with enhanced power density for heating and cooling requirements for a wide range of applications.

Acknowledgments

The authors gratefully acknowledge the support of Advanced Research Projects Agency-Energy (ARPA-E HEATS Program, Award DE-AR0000185) with Dr. Ravi Prasher and Dr. James Klausner as program managers. The authors would also like to acknowledge the support of Massachusetts Institute of Technology Energy Initiative and Massachusetts Clean Energy Center. HK acknowledges support from the Samsung scholarship. SNS and ENW also acknowledge the support of International Copper Association.

Appendix A. Supplementary material

Supplementary data associated with this article can be found, in the online version, at http://dx.doi.org/10.1016/j.apenergy.2016.12.003.

References

[1] International Energy Agency. Technology roadmap - energy efficient buildings: heating and cooling equipment. Paris, France; 2011.
[2] Mitchell JV. A new era for oil prices; 2006.
[3] de Almeida P, Silva PD. The peak of oil production—timings and market recognition. Energy Policy 2009;37(4):1267–76.
[4] Dunn S. Hydrogen futures: toward a sustainable energy system. Int J Hydrogen Energy 2002;27(3):235–64.
[5] Zalba B, Marín JM, Cabeza LF, Mehling H. Review on thermal energy storage with phase change: materials, heat transfer analysis and applications. Appl Therm Eng 2003;23(3):251–83.
[6] Veerappan M, Kalaiselvam S, Iniyan S, Goic R. Phase change characteristic study of spherical PCMs in solar energy storage. Sol Energy 2009;83(8):1245–52.
[7] Farid MM, Khudhair AM, Razack SAK, Al-Hallaj S. A review on phase change energy storage: materials and applications. Energy Convers Manage 2004;45(9–10):1597–615.
[8] Kenisarin M, Mahkamov K. Solar energy storage using phase change materials. Renew Sustain Energy Rev 2007;11(9):1913–65.
[9] Sharma A, Tyagi VV, Chen CR, Buddhi D. Review on thermal energy storage with phase change materials and applications. Renew Sustain Energy Rev 2009;13(2):318–45.
[10] Pardo P, Deydier A, Anxionnaz-Minvielle Z, Rougé S, Cabassud M, Cognet P. A review on high temperature thermochemical heat energy storage. Renew Sustain Energy Rev 2014;32:591–610.
[11] N'Tsoukpoe KE, Liu H, Le Pierrès N, Luo L. A review on long-term sorption solar energy storage. Renew Sustain Energy Rev 2009;13(9):2385–96.
[12] Gur I, Sawyer K, Prasher R. Searching for a better thermal battery. Science (80-.) 2012;335(6075):1454–5.
[13] Tatsidjodoung P, Le Pierrès N, Luo L. A review of potential materials for thermal energy storage in building applications. Renew Sustain Energy Rev 2013;18:327–49.
[14] van Essen VM, Zondag Ha, Schuitema R, van Helden WGJ, Rindt CCM. Materials for thermochemical storage: characterization of magnesium sulfate. Proc Eurosun 2008:4–9.
[15] Chan CW, Ling-Chin J, Roskilly AP. A review of chemical heat pumps, thermodynamic cycles and thermal energy storage technologies for low grade heat utilisation. Appl Therm Eng 2013;50(1):1257–73.
[16] Sharafian A, Bahrami M. Assessment of adsorber bed designs in waste-heat driven adsorption cooling systems for vehicle air conditioning and refrigeration. Renew Sustain Energy Rev 2014;30:440–51.
[17] Yeo THC, Tan IAW, Abdullah MO. Development of adsorption air-conditioning technology using modified activated carbon – a review. Renew Sustain Energy Rev 2012;16(5):3355–63.
[18] Fernandes MS, Brites GJVN, Costa JJ, Gaspar AR, Costa VAF. Review and future trends of solar adsorption refrigeration systems. Renew Sustain Energy Rev 2014;39:102–23.
[19] Goyal P, Baredar P, Mittal A, Siddiqui AR. Adsorption refrigeration technology – an overview of theory and its solar energy applications. Renew Sustain Energy Rev 2016;53:1389–410.
[20] Suzuki M. Application of adsorption cooling systems to automobiles. Heat Recover Syst CHP 1993;13(4):335–40.
[21] Pang SC, Masjuki HH, Kalam MA, Hazrat MA. Liquid absorption and solid adsorption system for household, industrial and automobile applications: a review. Renew Sustain Energy Rev 2013;28:836–47.
[22] Wang DC, Li YH, Li D, Xia YZ, Zhang JP. A review on adsorption refrigeration technology and adsorption deterioration in physical adsorption systems. Renew Sustain Energy Rev 2010;14(1):344–53.
[23] Askalany AA, Salem M, Ismail IM, Ali AHH, Morsy MG. A review on adsorption cooling systems with adsorbent carbon. Renew Sustain Energy Rev 2012;16(1):493–500.
[24] Shmroukh AN, Ali AHH, Ookawara S. Adsorption working pairs for adsorption cooling chillers: a review based on adsorption capacity and environmental impact. Renew Sustain Energy Rev 2015;50:445–56.
[25] Li XH, Hou XH, Zhang X, Yuan ZX. A review on development of adsorption cooling - novel beds and advanced cycles. Energy Convers Manage 2015;94:221–32.
[26] Hamdy M, Askalany A, Harby K, Kora N. An overview on adsorption cooling systems powered by waste heat from internal combustion engine. Renew Sustain Energy Rev 2015;51:1223–34.
[27] De Boer R, Smeding S, Mola S. Silicagel-water adsorption cooling prototype system for mobile air conditioning. In: Heat powered cycles Conf. Berlin, 7–9 Sept, no. August.
[28] Wang BK, Vineyard EA. Adsorption refrigeration. ASHRAE J 2011:14–24. no. September.
[29] Zhong Y, Wert K, Fang T. An adsorption air-conditioning system to reduce engine emissions and fuel consumption for heavy-duty vehicles. Int Refrig Air Cond Conf Purdue 2010;2000:1–8.
[30] Critoph RE. Adsorption refrigerator using monolithic carbon-ammonia pair. Int J Refrig 1997;20(2):146–55.
[31] Wang D, Zhang J, Tian X, Liu D, Sumathy K. Progress in silica gel-water adsorption refrigeration technology. Renew Sustain Energy Rev 2014;30:85–104.
[32] Henninger SK, Munz G, Ratzsch KF, Schossig P. Cycle stability of sorption materials and composites for the use in heat pumps and cooling machines. Renew Energy 2011;36(11):3043–9.
[33] Ge TS, Dai YJ, Wang RZ. Review on solar powered rotary desiccant wheel cooling system. Renew Sustain Energy Rev 2014;39:476–97.
[34] Sarbu I, Sebarchievici C. General review of solar-powered closed sorption refrigeration systems. Energy Convers Manage 2015;105:403–22.
[35] Al-Alili A, Hwang Y, Radermacher R. Review of solar thermal air conditioning technologies. Int J Refrig 2014;39:4–22.
[36] Best R, Rivera W. A review of thermal cooling systems. Appl Therm Eng 2015;75:1162–75.
[37] Bataineh KM, Alrifai S. Recent trends in solar thermal sorption cooling system technology. Adv Mech Eng 2015;7(5):1–20.
[38] Henninger SK, Jeremias F, Kummer H, Janiak C. MOFs for use in adsorption heat pump processes. Eur J Inorg Chem 2012;16:2625–34.

[39] Li X, Narayanan S, Michaelis VK, Ong T-C, Keeler EG, Kim H, et al. Zeolite Y adsorbents with high vapor uptake capacity and robust cycling stability for potential applications in advanced adsorption heat pumps. Microporous Mesoporous Mater 2015;201(5):151–9.
[40] Pino L, Aristov YI, Cacciola G, Restuccia G. Composite materials based on zeolite 4A for adsorption heat pumps. Adsorption 1997;3(1):33–40.
[41] Sultan M, El-Sharkawy II, Miyazaki T, Saha BB, Koyama S. An overview of solid desiccant dehumidification and air conditioning systems. Renew Sustain Energy Rev 2015;46:16–29.
[42] Douss N, Meunier F. Experimental study of cascading adsorption cycles. Chem Eng Sci 1989;44(2):225–35.
[43] Critoph RE. The use of thermosyphon heat pipes to improve the performance of a carbon-ammonia adsorption refrigerator. Int J Environ Conscious Des Manuf 2000;9(3):3–10.
[44] Li X, Narayanan S, Michaelis VK, Ong T-C, Keeler EG, Kim H, et al. Zeolite y adsorbents with high vapor uptake capacity and robust cycling stability for potential applications in advanced adsorption heat pumps. Microporous Mesoporous Mater 2015;201(C).
[45] Furukawa H, Gándara F, Zhang Y-B, Jiang J, Queen WL, Hudson MR, et al. Water adsorption in porous metal-organic frameworks and related materials. J Am Chem Soc 2014;136(11):4369–81.
[46] Taylor P, Lavagne d'Ortigue O, Trudeau N, Francoeur M. Energy efficiency indicators for public electricity production from fossil fuels. no. July, p. 23, 2008.
[47] Vaninsky A. Efficiency of electric power generation in the United States: analysis and forecast based on data envelopment analysis. Energy Econ 2006;28(3):326–38.
[48] Narayanan S, Yang S, Kim H, Wang EN. Optimization of adsorption processes for climate control and thermal energy storage. Int J Heat Mass Transf 2014;77:288–300.
[49] Kline SJ, McClintock FA. Describing uncertainties in single-sample experiments. Mech Eng 1953;75(1):3–8.
[50] Sircar S, Hufton JR. Why does the linear driving force model for adsorption kinetics work? Adsorption 2000;6(2):137–47.
[51] Dubinin MM. The potential theory of adsorption of gases and vapors for adsorbents with energetically nonuniform surfaces. Chem Rev 1960;60 (2):235–41.
[52] Kapoor A, Ritter J, Yang R. On the Dubinin-Radushkevich equation for adsorption in microporous solids in the Henry's law region. Langmuir 1989;5:1118–21.
[53] Incropera FP, DeWitt DP, Bergman TL, Lavine AS. Fundamentals Heat Mass Trans 2007.
[54] Furukawa H, Cordova KE, O'Keeffe M, Yaghi OM. The chemistry and applications of metal-organic frameworks. Sci (Washington, DC, U. S.) 2013;341(6149):974.